# The Kinetics of Binding Human Prolactin, but Not Growth Hormone, to the Prolactin Receptor Vary over a Physiologic pH Range†

Camille Keeler,‡ Elizabeth M. Jablonski,§ Yvonne B. Albert,§ Branden D. Taylor,‡ David G. Myszka,|| Charles V. Clevenger,§ and Michael E. Hodsdon*,‡

*Department of Laboratory Medicine, Yale University, New Haven, Connecticut 06520, Department of Pathology, Northwestern University, Chicago, Illinois 60611, and Center for Biomolecular Interaction Analysis, University of Utah, Salt Lake City, Utah 84132*

*Received September 20, 2006; Revised Manuscript Received December 20, 2006*

ABSTRACT: A member of the family of hematopoietic cytokines, human prolactin (hPRL) serves a dual role both as an endocrine hormone and as an autocrine/paracrine cytokine or growth factor. During investigation of the solution structural properties of hPRL, we have noted a surprising pH dependence of its structural stability over a range from approximately pH 6.0 to pH 8.0. An analysis of backbone atom NMR chemical shift changes and backbone amide hydrogen−deuterium exchange rates due to titration of the solution pH over this same range, along with calculations of protein surface electrostatic potential, suggests the possible involvement of a localized cluster of three His residues (27, 30, and 180), which comprise a portion of the high-affinity receptor-binding epitope. Surface plasmon resonance analysis of the interaction between hPRL and the extracellular domain (ECD) of the hPRL receptor reveals a selective 500-fold change in the dissociation rate between pH 8.3 and pH 5.8. In comparison, the interaction of hGH with the same receptor ECD did not demonstrate any significant dependence on pH. We also present an initial investigation of the pH dependence of hPRL function in rat Nb2 cell proliferation assays and a STAT5 luciferase gene reporter assay in the T47D human breast cancer cell line, whose results are consistent with our biophysical studies. The potential implications of this variation in hPRL's structural stability and receptor-binding kinetics over this physiologic range of pH are discussed.

Human prolactin (hPRL)[1] is a 23 kDa protein hormone closely related, both functionally and evolutionarily, to human growth hormone (hGH) and placental lactogen. Together, these three hormones are part of the larger family of hematopoietic cytokines, which contains erythropoietin, granulocyte-colony stimulating factor, interleukin-6, interleukin-4, and others. Proteins in this family share a common structural fold and recognize a conserved family of cell-surface receptors (*1*). Although best known for its traditional role as a pituitary-derived hormone, recent research has established important autocrine/paracrine functions of hPRL in the growth and development of a diversity of tissues (*2*). Multiple breast and prostate cancer cell lines express hPRL and its cell-surface receptor (hPRLr) (*3*−*5*). hPRL has mitogenic and angiogenic functions in these tumors and increases cancer cell motility (*6*, *7*). The biology of peripheral hPRL synthesis is distinct from the pituitary, including alternative mechanisms for transcriptional regulation, RNA splicing, and hormone storage and secretion (*8*). Whereas a majority of pituitary-derived PRL is secreted as the full-length, unmodified protein, glycosylated, phosphorylated, and proteolytically cleaved variants of PRL have been identified (*9*). Research has demonstrated functional consequences of these modifications, some of which may act to counter the tumorigenic effects of native hPRL (*10*−*15*).

We originally determined the solution structure of hPRL using NMR spectroscopy (*16*) and confirmed that the hormone adopts the conserved topology of the hematopoietic cytokines, consisting of four primary α-helices bundled together lengthwise. The helices span 25−32 residues in length and are interrupted by two stretches of residues, one between the first and second helices and another between the third and fourth helices, which correspond to the two long loops necessary for the "up−up down−down" topology of the four-helical bundle. These two long loops were demonstrated to be highly dynamic and mostly unstructured in solution according to an analysis of their backbone atom NMR chemical shifts and NMR relaxation rates. Experimentally, structure determination was frustrated by multiple technical limitations including reversible oligomerization of the hormone in solution resulting in low signal to noise and broad line widths of NMR signals. Recently, a greatly improved solution structure of hPRL was reported (*17*) where

† This work was supported by National Institutes of Health Grants R01 CA108992-01 (M.E.H.), R01 CA69294 (C.V.C.), R01 CA102682 (C.V.C.) and a grant from the Charlotte Geyer Foundation (M.E.H.).

* Address correspondence to this author. Tel: 203-737-2674. Fax: 203-688-8704. E-mail: michael.hodsdon@yale.edu.

‡ Yale University.

§ Northwestern University.

|| University of Utah.

[1] Abbreviations: hPRL, human prolactin; hGH, human growth hormone; NMR, nuclear magnetic resonance; PRLr, prolactin receptor; ECD, extracellular domain; Ser, serine; Asp, aspartate; Glu, glutamate; PFG, pulsed field gradients; DSS, 2,2-dimethyl-2-silapentane-5-sulfonate sodium salt; ppm, part per million; HSQC, heteronuclear single-quantum coherence; 2D, two dimensional; 3D, three dimensional; His, histidine; HX, hydrogen−deuterium exchange; SPR, surface plasmon resonance.

10.1021/bi061958v CCC: $37.00 
Published on Web 02/06/2007

the investigators overcame these technical problems through the use of a higher field (800 MHz) NMR spectrometer, incorporation of a new class of NMR structural restraints known as residual dipolar couplings, and altered solution conditions (pH 8.0 and 37 °C) where reversible oligomerization of the hormone is minimized. This newly reported solution structure of hPRL represents an improvement over our original model and clarifies subtle structural features of the hormone. All results reported in the current publication are interpreted using this updated structural model.

During our ongoing investigations into the structural properties of hPRL, we have noted an unexpected pH dependence to its stability over the physiologic range of approximately 6.0−8.0. Associated with this change is a localized cluster of pH-dependent NMR chemical shift changes in the vicinity of hPRL's high-affinity receptor-binding site. Therefore, we hypothesize that the functional properties of hPRL may be affected by solution acidity over this same pH range. This publication details the above observations and provides experimental support for our hypothesis.

## MATERIALS AND METHODS

*Recombinant Protein Production.* hPRL was expressed recombinantly in the BL21(DE3) strain of *Escherichia coli* and purified from inclusion bodies as previously described (*16*). The cDNA for hGH subcloned into the modified pT7L vector used for hPRL expression was a generous gift of Dr. Priscilla Dannies. Recombinant hGH was expressed and purified similarly from inclusion bodies as hPRL. The cDNA for the hPRLr extracellular domain (ECD) was subcloned into the protein expression vector pET11b (Invitrogen). Expression, refolding, and purification of the hPRL receptor ECD followed a previously described protocol (*18*). Uniformly isotope-labeled protein was prepared similarly using commercial growth media (Spectra Stable Isotopes, Inc.), appropriately enriched either with $^{15}N$ alone or $^{13}C$ and $^{15}N$ together. For NMR spectroscopy, hPRL was concentrated to 1.0 mM (unless otherwise noted) and exchanged into 20 mM potassium phosphate buffer at a specified pH, 100 mM NaCl, 10% $D_2O$, 1 mM $NaN_3$, and 1 $\mu$M protease inhibitors leupeptin and pepstatin.

*Chemical Denaturation Monitored by Trp Fluorescence.* All denaturation experiments were performed at 25 °C with a Hitachi H-3010 fluorescence spectrophotometer. The protein samples were excited at 280 nm with 10 nm slit widths for excitation and emission. Samples were preequilibrated to 25 °C and maintained at this temperature in the fluorometer via a circulating water bath and stir bar assembly. Fluorescence emission was recorded at 325 nm using a 1 cm quartz cuvette. A potassium phosphate buffer system was employed for each denaturation experiment. Urea denaturation samples were prepared with a final protein concentration of approximately 2 $\mu$M. For most experiments conducted at a single pH, 23 samples were prepared in duplicate ranging from 0 to 9.9 M urea. Fresh 10 M urea stock solution was prepared for each denaturation experiment using either American Bioanalytical Ultra Pure urea or Sigma Aldrich SigmaUltra urea. Urea stock concentrations were determined via refractive index measurement from an Atago R5000 hand refractometer. Samples were typically allowed to equilibrate for 15 h at room temperature prior to the start of fluorescence measurements. Reversibility of protein unfolding was demonstrated by combining an aliquot of the protein with the concentrated urea stock solution, resulting in a final urea concentration greater than 8 M, and then subsequently diluting with buffer to a number of lower urea concentrations to allow refolding. Trp fluorescence in these refolded samples was compared to the fitted denaturation curves (described below), and all agreed within 10%. All stock solutions were filtered through a 0.2 $\mu$m filter prior to sample preparation.

The chemical denaturation curves were analyzed using the SigmaPlot software package from SPSS Inc. (Chicago, IL). Standard deviations for each Gibbs free energy calculation were based on the program's reported standard error of the estimate and should be considered a rough error analysis. A sigmoidal curve was fit to each set of denaturation data points using a nonlinear least-squares algorithm and the equation (*19*):

$$y = \frac{(y_F + m_F[D]) + (y_U + m_U[D])e^{m(([D]-[D]_{1/2})/RT)}}{1 + e^{m(([D]-[D]_{1/2})/RT)}}$$

where $m$, $m_F$, and $m_U$ are the slopes at the curve midpoint, start, and end point, respectively, $y_F$ and $y_U$ are the curve maximum and minimum, and [D] and [$D_{1/2}$] are the denaturant concentration and the denaturant concentration at the curve midpoint. The Gibbs free energy of unfolding was then calculated from

$$\Delta G_U = m[D]_{1/2}$$

*NMR Spectroscopy.* All NMR experiments were collected on a Varian INOVA 600 MHz spectrometer using a 5 mm triple resonance (HCN) room temperature probe equipped with triple axis (XYZ) pulsed magnetic field gradients (PFGs) and utilized pulse sequences from the Varian BioPack User Library. Backbone and aliphatic side-chain resonance assignments were determined starting with previously reported assignments (*16*) and extended using additionally collected HNCO, HN(CO)CA, and HNCACB 3D NMR experiments. All NMR spectra were processed using NMRPipe (*20*), with subsequent display and analysis in SPARKY (*21*). Chemical shifts were referenced indirectly to DSS at 0.00 ppm, with heteronuclear dimensions referenced using their relative gyromagnetic ratios (*22*).

*Measurement of Amide Hydrogen−Deuterium Exchange (HX) Rates*. Amide deuterium exchange for uniformly $^{15}N$-labeled hPRL was monitored at 25 °C via cross-peaks in 2D $^1H-^{15}N$ HSQC NMR spectra. Fully protonated protein was exchanged into buffered $D_2O$ using Bio-Rad Micro Bio-Spin 6 chromatography columns. Each column was preequilibrated with buffered $D_2O$, loaded with 75 $\mu$L of approximately 0.5−1 mM protein, and centrifuged at 1000*g* for 4 min to recover the solvent-exchanged protein. Immediately following $D_2O$ buffer exchange, sequential $^1H-^{15}N$ HSQC NMR spectra would be collected with the earliest experiments using 16 transients for the initial time points, which increased to a maximum of 128 transients during the course of the experiment as the NMR signal was lost due to exchange. All $D_2O$ buffers were prepared from Aldrich 99.9% deuterium oxide and 1 M buffer stocks leaving the final concentration of $D_2O$ at approximately 97%. All pH

values were monitored using a calibrated Fischer pH digital meter with combination electrode and corrected for measurements in $D_2O$: pD = pH + 0.4 (*23*). In cases where the aforementioned spin-column method yielded poor-quality $^1H-^{15}N$ HSQC NMR spectra, a rapid-dilution method was employed. In the rapid-dilution method, fully protonated protein concentrated to approximately 1 mM would simply be added to $D_2O$ buffered at the appropriate pH to make a sample of approximately 400 $\mu$M protein, with a final $D_2O$ content of 65%. The NMR spectra would then be collected as described earlier.

*Measurement of Receptor-Binding Kinetics for hPRL and hGH by Surface Plasmon Resonance (SPR).* SPR experiments were done on a Biacore T100 (Biacore AB, Uppsala, Sweden). The hPRLr-ECD was minimally biotinylated using sulfo-NHS-LCLC-biotin and then captured onto a streptavidin sensor chip. Three different surface densities of the ECD were created at ~350, 120, and 50 RU. Ligand binding data were collected at five concentrations in a 3-fold dilution series. The high concentration was 380 nM for pH 8.3, 7.8, and 7.3 and 1140 nM for pH 6.8, 6.3, 5.8, and 5.3. Each concentration was tested in duplicate over the three different density surfaces. The running buffer contained 25 mM potassium phosphate and 50 mM NaCl, with 0.005% p20 and 0.l mg/mL BSA. The buffer included 50 $\mu$M $ZnCl_2$ for the studies involving hGH. Bound complexes were regenerated with a 5 s pulse of 1/1000 dilution of phosphoric acid. The samples were tested from low pH to high pH. All of the response data from the three density surfaces were globally fit to a 1:1 interaction model (A + B = AB) to extract the rate constants at 25 °C using the software program Scrubber-2 (Biologic Software Pty Ltd., Australia).

*Nb2 Lymphoma Cell Proliferation Assay*. Nb2-11C cells were maintained in RPMI 1640 and supplemented with additional L-glutamine (Mediatech, Inc., no. 10-040-CV), 10% fetal bovine serum, 10% gelding serum, 0.1 mM 2-mercaptoethanol, and 1% penicillin−streptomycin solution. To assess the ability of hPRL to stimulate Nb2 cell proliferation in the presence of differing pH values (5.0−8.0), $5 \times 10^4$ Nb2 cells were aliquoted in triplicate wells in the medium described above with 0.1% BSA substituted for the above serum, and the pH was adjusted as indicated with 10 M HCl. Increasing concentrations (0.1−100 ng/well) of hPRL were added in the pH-adjusted medium and the cells incubated for 48 h. Cells were then pulsed with 1 $\mu$Ci of [$^3$H]thymidine at 37 °C for 4 h. The incorporation of radiolabel was determined by scintillography of the harvested, washed cells. To ensure that the differences in proliferation were not due to excessive cell death secondary to low pH, Nb2 cells were plated as described above and incubated in medium with or without serum (at the varying pH ranges); cells were then assessed for viable cell number with trypan blue hemocytometry and radiolabeled as above. Statistical analysis was generated by two-way ANOVA (Bonferroni post-hoc test), and data are representative of one of three experiments, each of which included triplicate data points.

*STAT5 Gene Reporter Assay.* The luciferase reporter construct LHRE-TK-Luc containing multimerized STAT5 DNA-binding sites was a kind gift of R. J. M. Ross (Sheffield University, Sheffield, U.K.). T47D cells were cultured and transfected as previously described (*24*) with 1.0 $\mu$g of LHRE-TK-Luc and 0.25 $\mu$g of a control *Renilla* luciferase reporter construct. Twenty-four hours after transfecting cells, the medium was changed to BSA-only containing medium with the pH adjusted as above and cultured for an additional 24 h. Cells were then treated with increasing concentrations of hPRL (0−500 ng/mL) and dexamethasone (100 ng/mL) in pH-adjusted medium for 24 h. Luciferase assays were conducted by standard methods using the dual luciferase assay system (Promega) and a Victor$^3$V plate-reading luminometer (Perkin-Elmer). Statistical analysis was generated by two-way ANOVA (bonferroni post-hoc test), and data are representative of one of three experiments conducted with triplicate transfections.

## RESULTS

*Chemical Denaturation of hPRL and hGH.* Figure 1A presents urea denaturation curves for hPRL and hGH at a variety of pH values. A least-squares method was used to fit a sigmoidal curve to each unfolding data set in Figure 1A, as detailed in Materials and Methods. The Gibbs free energies of unfolding were calculated from each fitted curve and are also reported in the figure. The global stability of hPRL is clearly pH-dependent, as is visible from both the fitted free energies of unfolding and the shifts in the midpoints of the denaturation curves as the pH is increased from 6.0 to 8.0. As a comparison, we also monitored equilibrium unfolding for hGH at both pH 6.0 and pH 8.0 and found a dramatically higher stability for this protein (see Figure 1). Because a post-unfolding baseline could not be observed for the hGH transition in urea, we repeated the chemical denaturation experiments in guanidine hydrochloride (GuHCl). A reproducible pre-unfolding transition was observed for hGH in GuHCl, which complicated fitting of the data to extract reliable free energies of unfolding. This early transition may represent a conformational change induced by low concentrations of GuHCl. Consequently, the unfolding free energies for hGH reported in Figure 1 have large standard errors and should be interpreted cautiously. However, we note that our derived values of 15.5 and 13.3 kcal/mol for unfolding of hGH at pH 8 during urea and GuHCl unfolding, respectively, agree well with the previously published value of 15 kcal/mol (*25*).

The pH dependence of the Gibbs free energies of unfolding for hPRL and hGH is displayed in Figure 2. A trend toward decreased stability at lower pH values is evident for hPRL. In contrast, the stability of hGH appears to increase slightly in its stability at pH 6 compared to pH 8, which is supported by the relative midpoints of the transitions in both the urea and GuHCl denaturation curves. Overall, the changes in $\Delta G_{unf}$ and the shifts in unfolding midpoints are larger, on a relative basis, for hPRL compared to hGH. Note that multiple "refolding" points were included in all of the denaturation experiments, demonstrating reversibility of unfolding across the transition, as detailed in Materials and Methods.

*Localized Changes in the hPRL Backbone NMR Chemical Shifts Due to Changes in pH.* The NMR chemical shifts for the backbone amide $^1H$, $^{15}N$, and carbonyl $^{13}C$ atoms were measured for hPRL across a range of pH values. Figure 3A illustrates the chemical shift differences that accompany titration of the solution conditions from low to high pH. The largest perturbations occur at or near His residues at positions

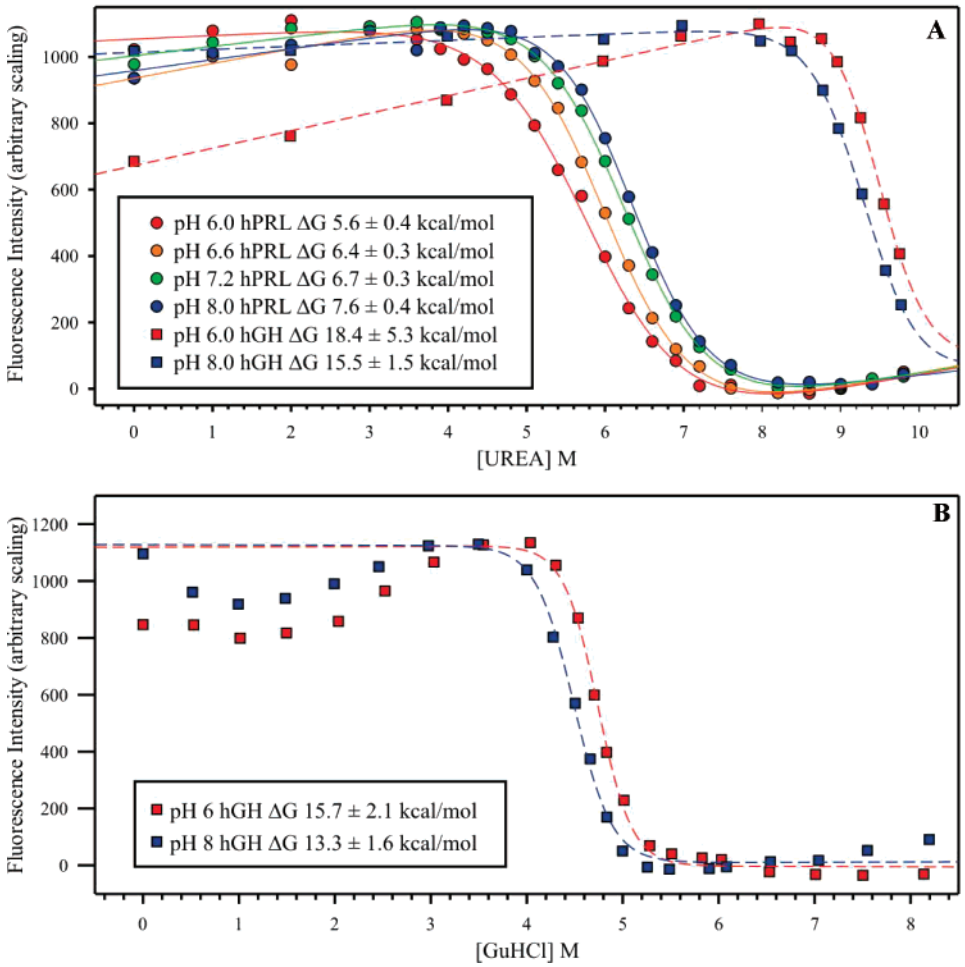


FIGURE 1: Fluorescence-detected chemical denaturation curves for hPRL and hGH as a function of pH. (A) Urea-induced unfolding of both hPRL and hGH with pH values as indicated in the legend. Each data set was fitted to a sigmoidal curve (see Materials and Methods), which was used to determine a Gibbs free energy of unfolding for each condition (reported in the legend). (B) Because complete unfolding could not be observed for hGH during urea denaturation, the unfolding titration was repeated using guanidine hydrochloride (GuHCl) as the denaturant.

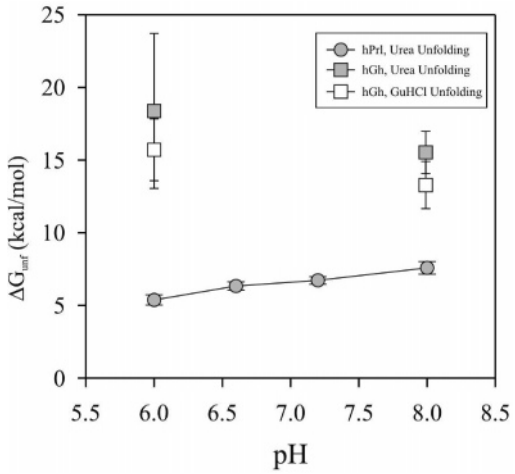


FIGURE 2: Gibbs free energy of unfolding measured by chemical denaturation (displayed in Figure 1) for hPRL and hGH as a function of pH.

27, 30, 46, 59, 97, 138, 173, 180, and 195. The relative positions of the helices and His residues for the hPRL tertiary structure are shown above the bar graphs as shaded rectangles and marked by "H", respectively. Recombinant hPRL has an experimentally determined p*I* of 6.2 (*26*), implying net negative and positive charges at pH values above and below this value, respectively. A net negative charge for hPRL at pH 7 and higher is supported by our experience where hPRL binds tightly to anion-exchange (i.e., net positively charged) matrices, whereas it does not bind at pH 6.0 or lower. Over the pH range investigated, we expect for the imidazole side chains of His residues to be the major titratable groups in hPRL and, hence, largely responsible for the net change in overall charge and global stability.

The NMR chemical shift of an atom serves as a sensitive indicator of its local chemical environment, and thus, perturbations in NMR chemical shifts can be used to identify localized chemical or structural changes, which may be static or dynamic in nature. Mapping of backbone atom NMR chemical shift changes to the tertiary structure of hPRL in Figure 4A identifies the structural perturbations due to titration of the solution pH from 8.0 to 6.0, with the location of His side chains noted for comparison. There is a diffuse scattering of chemical shift changes throughout the protein structure with a rough correlation to the location of His side chains (this correlation is also visible along the primary sequence in Figure 3). However, most notable in both Figures 3 and 4A is a concentration of the largest chemical shift changes in the vicinity of three His residues (27, 30, and 180), which are clustered structurally on the "front" face of the protein in the interface between the first and fourth

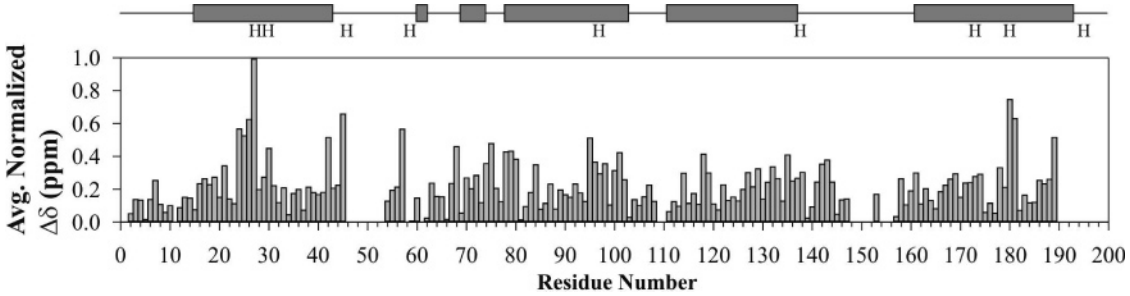


FIGURE 3: Changes in NMR chemical shifts for the backbone atoms of hPRL due to lowering of the solution pH from 8.0 to 6.0. Chemical shift changes for the backbone amide $^{1}H$, $^{15}N$, and carbonyl $^{13}C$ atoms were normalized by the widths of their typical distributions in proteins ($10 \times {}^{1}H_{\delta} = 1.5 \times {}^{13}C_{\delta} = 1 \times {}^{15}N_{\delta}$, in ppm), averaged, and plotted on a per-residue basis. The location of helices (shaded bars) and His residues (H) in the PRL sequence is illustrated at the top of the figure.

helices. We note that the high-affinity binding site for the hPRL receptor overlaps with this cluster of His side chains.

In order to better understand the consequence of protonating His residues in hPRL, we separately calculated the surface electrostatic potentials of the protein both assuming that all His residues are neutral (Figure 4B) and also assuming that all His residues are protonated and positively charged (Figure 4C). In Figure 4B, representing what might be expected for hPRL at a high pH, electrostatic potential is patchily distributed across the protein surface with an apparent slight excess of negatively charged surface as would be expected from its reported p*I* of 6.2 and its high affinity for anion-exchange columns at this pH. On the other hand, in Figure 4C, representing what *might* be expected for hPRL at low pH, a large, contiguous concentration of positive charge is now visible on the front face of the protein, with only minimal changes in electrostatic potential found on the back side of the protein compared to higher pH. It is important to note that this calculation of electrostatic potential is based upon "standard" p$K_a$ values for all of the ionizable groups and is only meant to demonstrate the general importance of the clustered positively charged residues on the front face of the protein. It is likely that a number of these residues will display aberrant p$K_a$ values, which will contribute dramatically to its pH-dependent behavior (*27*). It will be important in future studies to directly measure the protonation state of all of the ionizable groups in hPRL and derive their true p$K_a$ values, which will then allow a more exact understanding of the mechanism for the pH dependence of its stability.

*Monitoring of Residue-Specific Backbone Amide Hydrogen−Deuterium Exchange Rates in hPRL*. The structural stability and flexibility of the polypeptide backbone can be characterized by analysis of residue-specific amide hydrogen−deuterium exchange (HX) rates (*28*, *29*). Hydrogen bonding between backbone amides and carbonyls, characteristic of ordered protein secondary structure, greatly slows the chemical exchange of amide hydrogens with solvent, whereas entirely unstructured regions lack hydrogen bonds and display rapid exchange rates. The degree of conformational flexibility within the polypeptide backbone, manifested by opening and closing reactions of local hydrogen-bonded structure, can be described by comparison of amide hydrogen exchange rates along the protein sequence, using a protocol pioneered by Englander and colleagues (*30*) (outlined in the Appendix). The application of this model to scientific investigations of protein stability and function has been nicely reviewed (*31*, *32*).

Residue-specific backbone HX rates were measured for hPRL across a range of pH values. Analysis of the derived exponential rate constants for individual residues requires interpretation of whether exchange is occurring in the so-called $EX_1$ or $EX_2$ limits, which is theoretically based on the relative magnitudes of the intrinsic ("random coil") exchange rate for each residue and the rate of its closing reaction to form a hydrogen-bonded conformation (see the Appendix for a detailed description). A common method for characterizing these limits of exchange behavior is to monitor the measured exchange rate for each residue as a function of pH, based upon the assumption that small changes in pH around physiological conditions (i.e., in the range of pH 6−8) will only affect the intrinsic exchange rates for the unfolded polypeptide without perturbing the stability of the protein. Unfortunately, for PRL this assumption does not apply as Figures 1 and 2 clearly demonstrate a strong dependence of hPRL global stability on pH. Therefore, as detailed in the Appendix, we are only able to assert that, at higher pH values around 7.5−8.0, measured HX rates for PRL appeared to approach the $EX_1$ limit, where they show no direct dependence on pH and approximate the local rates of structural opening. Conversely, at low pH values around 6.0−6.6, exchange approximated $EX_2$ behavior, where the measured HX rates for individual residues depended linearly on pH and when normalized to their intrinsic chemical rates for exchange provided the equilibrium constant (and corresponding Gibbs free energy) for the opening and closing reaction of the localized hydrogen-bonded structure (known as $\Delta G_{HX}$).

Our interpretation of the residue-specific amide HX exchange rates for hPRL is depicted in Figure 5 and summarized in Table 1 as averages of $\Delta G_{HX}$ or $\log(k_{ex})$ values at pH 6.6 and 8.0, respectively, for each of the long helices and the receptor-binding minihelix in hPRL. In general, faster exchanging residues are colored red in Figure 5, and slower exchanging residues are in blue. Some amide hydrogens exchange so quickly with the deuterated solvent that their NMR peaks are lost entirely within the dead time of the experiment (~10 min); such residues are considered to have very fast amide HX rates and are colored red. At pH 6.0, where amide HX in hPRL appears to follow $EX_2$ behavior, the Gibbs free energies for the equilibrium between the localized open and closed states for each residue have been mapped onto the hPRL structure in Figure 5A. At pH 8.0, where the $EX_1$ limit for hPRL HX was assumed, the negative logs of the measured exchange rates have been mapped onto the ribbon diagram in Figure 5B, which approximate the opening rates for local structural fluctuations.

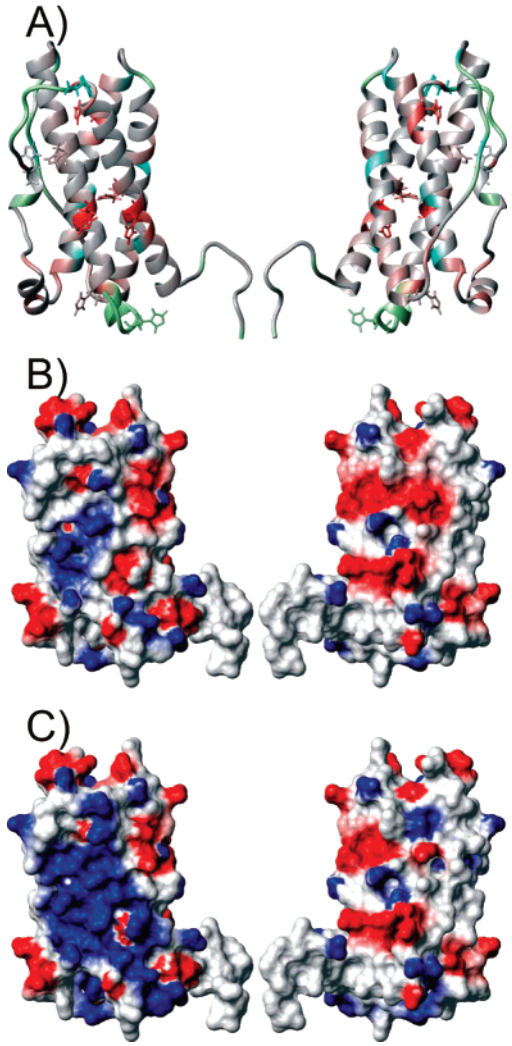


FIGURE 4: (A) The hPRL backbone ribbon (PDB code 1RW5) is colored from blue-gray to red according to the average chemical shift perturbations defined in Figure 3, with the largest changes rendered in red; the side chains of all the His residues are also shown and colored similarly to the backbone. Residues with missing backbone assignments at both pH 6.0 and pH 8.0 are colored light green, and residues assigned at pH 8.0 and missing at pH 6.0 are colored turquoise. In both (B) and (C) the surface electrostatic potential for 1RW5 was calculated using MOLMOL and mapped onto the molecular surface, with coloring in shades of red representing negative potential (e/Å, charge per distance) from −1.5 to −5.5 and shades of blue representing positive potential from 1.5 to 5.5. In (B) all His residues were considered unprotonated and neutral, whereas in (C) all His residues were considered protonated and positively charged. In both cases, Asp and Glu residues were considered unprotonated and negatively charged, and Arg and Lys residues were taken as protonated and positively charged. For each, the "front" face of the PRL structure, containing the high-affinity receptor-binding site, is displayed on the left, and the "back" face is shown on the right (rotated 180° along the vertical axis of the page).

A comparison of both diagrams in panels A and B of Figure 5 reveals that a majority of helical residues are well stabilized with slow relative exchange rates (blue). We note a general agreement of the average $\Delta G_{HX}$ for each long helix with the $\Delta G_{unf}$ for hPRL at pH 6.0 as measured by chemical denaturation in Figure 1. In contrast, residues in the two long loops and at the extrema of the long helices display faster exchange rates and $\Delta G_{HX}$ values much lower than the $\Delta G_{unf}$, implying a higher degree of structural flexibility in these

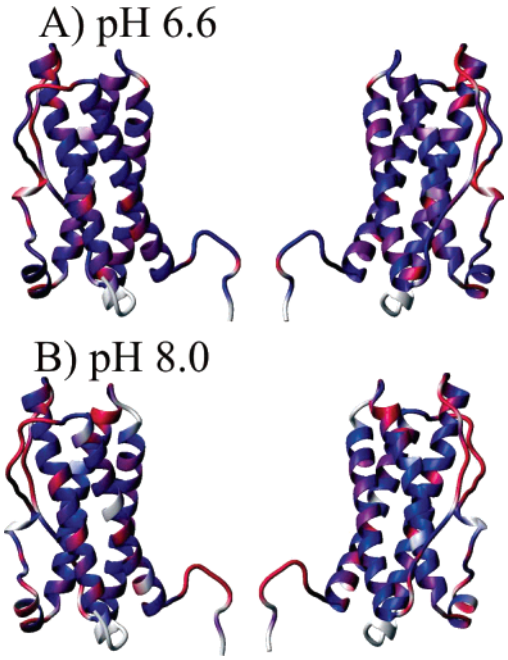


FIGURE 5: Backbone amide HX rates mapped onto ribbon diagrams of the human PRL (1RW5) tertiary structure, with the front and back faces of the protein displayed on the left and right, respectively. In the upper diagrams (A), residue-specific stabilities ($\Delta G_{HX}$ values) derived from HX rates acquired at pH 6.0 have been colored from red to blue, representing $\Delta G_{HX}$ values from 4.0 kcal/mol (or less) to 7.0 kcal/mol, respectively. In the lower diagrams (B), the logarithm of HX rates, approximating the $\log(k_{op})$ values, has been similarly colored from red to blue, representing values of 1 (or less) to 2, respectively. Prolines and residues with either overlapping or uncertain assignment have been colored gray.

Table 1: Average Backbone Amide HX Rates for Helices in hPRL

| | $\Delta G_{HX}$, pH 6.6, PRL (kcal/mol) | $\log(k_{ex})$, pH 8.0, WT PRL |
|---|---|---|
| helix 1 (14−43) | 5.8 | 2.7 |
| helix 2 (78−103) | 5.8 | 3.1 |
| helix 3 (111−137) | 5.6 | 3.1 |
| helix 4 (161−193) | 6.0 | 3.0 |
| minihelix (68−76) | 6.3 | 2.7 |

regions. Although the HX rates for a majority of residues in the two long loops are very fast relative to the helical bundle, there were still a surprising number of amides with relatively slow HX rates. Outside of the receptor-binding minihelix (approximately residues 67−73 in the first long loop), typical secondary structure-related hydrogen-bonding patterns have not been described for loop residues. It is possible the slowly exchanging residues are stabilized by long-range hydrogen bonds with the helical bundle or by interactions with side chains from nearby loop residues. However, the precise origin of the structural stabilization responsible for slowing the amide HX rates for these residues is currently unclear.

Interestingly, residues in the vicinity of three clustered His residues demonstrating the largest NMR chemical shift changes with pH (H27, H30, and H180) have aberrantly faster amide HX rates. As these residues are located in the middle of long α-helices, which would be expected to fold and unfold as single units, isolated increases in backbone amide HX rates are unexpected. It is not clear whether these faster HX rates are a consequence of increased structural fluctuations in this region or some alternative mechanism for catalysis of backbone amide HX, possibly due to the

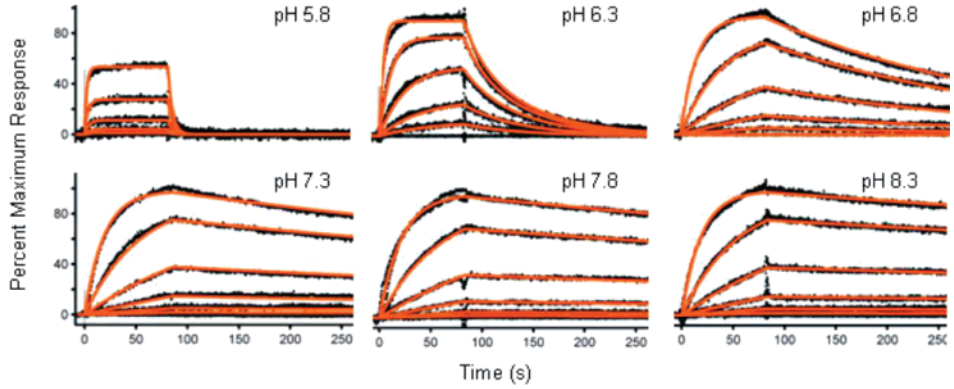


FIGURE 6: Representative surface plasmon resonance response curves for hPRL interacting with the immobilized hPRr-ECD as a function of pH. The results of global fits to the data for each pH condition are represented by solid lines. The pH dependence of the dissociation phase is evident in the curves.

imidazole side chains of the His residues. However, the remaining six His residues in hPRL, two of which are also located within long helices, do not display similar aberrant behavior. Therefore, we suspect that residues in the vicinity of H27, H30, and H180 are locally destabilized due to the unfavorable concentration of positive electrostatic potential displayed in Figure 4B. As differences in fast time scale (nanosecond to picosecond) dynamics for these residues were not detected in our previous analysis of hPRL backbone amide $^{15}$N NMR relaxation (*16*), the conformational fluctuations associated with this localized destabilization are most likely occurring on a slower (microsecond to second) time scale.

*Measurement of hPRL Receptor-Binding Kinetics for hPRL and hGH as a Function of pH.* Binding kinetics for interaction with the hPRL receptor ECD were measured by surface plasmon resonance using a Biacore T100. Minimally biotinylated receptor was captured onto a streptavidin sensor surface at three different densities. The interactions of both hPRL and hGH were studied from pH 5.8 to pH 8.3 in half-pH unit increments. The data at each pH from all three surface densities were globally fit to a simple bimolecular interaction model. Representative sensorgrams for hPRL demonstrating the quality of the data and fits are shown in Figure 6. The binding kinetics and calculated equilibrium dissociation constants are presented in Table 2. When the interaction rate constants are plotted graphically as in Figure 7, a dramatic trend in the data is apparent. The dissociation rate constant for hPRL is strongly dependent on pH, with an approximate 500-fold increase over the pH range of 8−6. However, there is less than a 1.2-fold change in the association rate for hPRL across this same pH range. In comparison, the kinetics of hGH's interaction with the hPRLr-ECD show very little dependence on pH. Because binding of hGH to the hPRLr-ECD requires the addition of 50 mM $ZnCl_2$, we compared the receptor-binding kinetics of hPRL in the presence and absence of $ZnCl_2$, at both pH 8.0 and pH 6.0 and found no significant changes due to the presence of $Zn^{2+}$. We interpret the above-described results as supporting the existence of a pH-dependent change in the structural or physicochemical properties of hPRL and *not* in hGH or the hPRLr-ECD.

*hPRL Stimulation of Rat Nb2 Lymphoma Cell Proliferation Is pH-Dependent.* In an initial attempt to correlate the above biophysical studies of hPRL behavior with its cellular function, the pH dependence of hPRL-induced proliferation of rat Nb2 cells was examined. Since its introduction in 1980 (*33*), this assay has served as a widely utilized standard "benchmark" for monitoring PRL function from a variety

Table 2: Binding Kinetics for Association of hPRL and hGH for Interaction with the hPRLr-ECD

| ligand | pH | measured association rate constant,[a] $k_a$ ($M^{-1}s^{-1}$) | measured dissociation rate constant,[a] $k_d$ ($s^{-1}$) | calculated equilibrium constant,[a] $K_d$ (nM) |
|---|---|---|---|---|
| hPRL | 8.3 | $1.398(6) \times 10^5$ | $6.2(3) \times 10^{-4}$ | 4.4(2) |
| hPRL | 7.8 | $1.229(7) \times 10^5$ | $8.4(4) \times 10^{-4}$ | 6.8(3) |
| hPRL | 7.3 | $1.421(7) \times 10^5$ | 0.00140(4) | 9.9(3) |
| hPRL | 6.8 | $1.658(7) \times 10^5$ | 0.00397(4) | 24.0(3) |
| hPRL | 6.3 | $1.79(1) \times 10^5$ | 0.0220(2) | 123(1) |
| hPRL | 5.8 | $2.31(6) \times 10^5$ | 0.230(4) | $1.00(4) \times 10^3$ |
| hGH | 8.5 | $3.478(5) \times 10^4$ | $2.3(1) \times 10^{-4}$ | 6.7(3) |
| hGH | 7.8 | $4.077(5) \times 10^4$ | $2.18(9) \times 10^{-4}$ | 5.3(2) |
| hGH | 7.3 | $4.266(8) \times 10^4$ | $2.0(2) \times 10^{-4}$ | 4.7(4) |
| hGH | 6.8 | $4.772(8) \times 10^4$ | $3.9(1) \times 10^{-4}$ | 8.1(3) |
| hGH | 6.3 | $4.151(5) \times 10^4$ | $4.1(1) \times 10^{-4}$ | 9.8(1) |
| hGH | 5.8 | $4.834(7) \times 10^4$ | $4.5(2) \times 10^{-4}$ | 9.4(4) |

[a] The number in parentheses represents the standard error in the last significant digit.

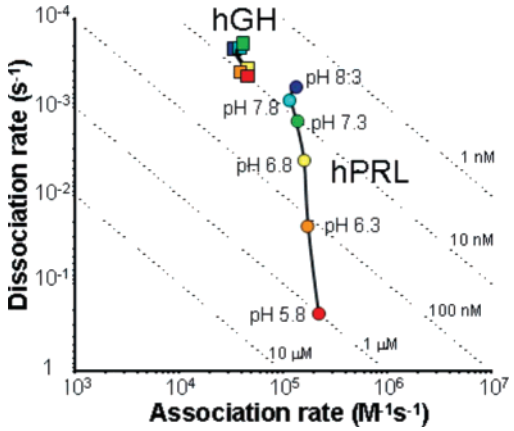


FIGURE 7: Comparison of the association and dissociation rate constants as a function of pH for the interactions of hPRL and hGH with the hPRLr-ECD as measured using SPR. Results for hPLR are shown as color-coded circles, and hGH data are represented by similarly colored squares. Dotted lines show the range of rate constants consistent with the indicated dissociation equilibrium constants.

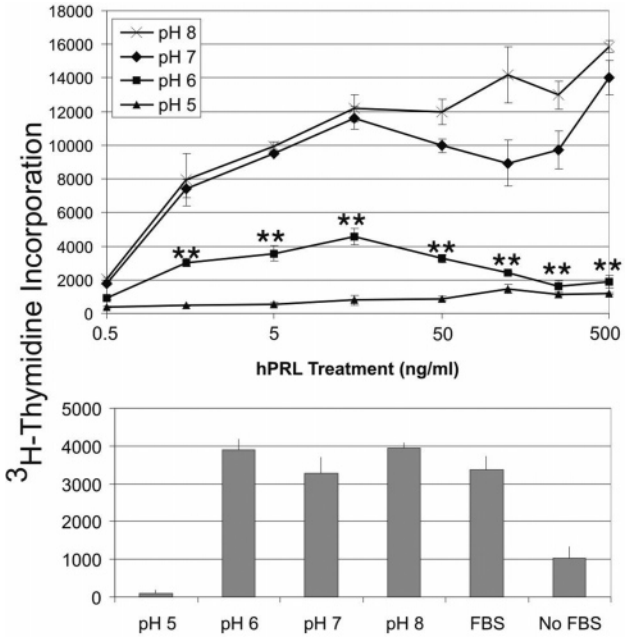


FIGURE 8: Rat Nb2 lymphoma cell proliferation as measured by [$^3$H]thymidine incorporation. Nb2 cell growth was stimulated by increasing concentrations of recombinant hPRL in pH-adjusted media (top panel). To ensure cells were not undergoing reduced proliferation secondary to the pH-adjusted media, Nb2 cells were cultured in the presence (pH 5.0−8.0 and FBS) or absence (no FBS) of serum, and proliferation was determined by [$^3$H]thymidine incorporation (bottom panel). Both the "FBS" and "no FBS" experiments were performed at pH 7.8. Reduced proliferation was only noted in FBS adjusted to pH 5.0. Error bars indicate ± the standard deviation of three independent replicates. ** indicates $p < 0.001$ statistical significance between pH 7/8 and pH 6 at 0.3−100.0 ng/mL doses.

of species. Nb2 cells treated in the presence of medium adjusted to pH 7.0 or 8.0 display a robust proliferation curve in response to increasing concentrations of hPRL (Figure 8, upper panel), with 5-fold increases in thymidine incorporation from 0 to 1 ng/well hPRL treatment and a plateau of response from 1 to 100 ng/mL. In contrast, cells treated in medium adjusted to pH 6.0 demonstrate a significantly diminished proliferation response, and cells treated in the presence of pH 5.0 showed no response. To ensure the decreased proliferation was not due to excessive cell death secondary to the decreased pH, Nb2 cells were also treated with pH-adjusted growth medium in the presence and absence of serum and assessed for thymidine incorporation and viability. As shown in the lower panel of Figure 8, there is no significant difference in the thymidine incorporation of cells grown in serum-containing medium adjusted to pH 6.0−8.0; however, a significant reduction in thymidine incorporation was noted at pH 5.0. In parallel, a significant decrease in cell viability was only noted at pH 5.0 (data not shown). Taken together, these results indicate that while Nb2 cells survive and respond well at pH 6.0 to serum, which contains other growth factors that can sustain Nb2 cell growth, a marked reduction in response occurs at pH 6.0 to stimulation with hPRL alone. Although it is possible that other potential experimental variables contribute to the observed pH dependence, these results are generally consistent with the biophysical behavior of hPRL and suggest the possibility of a dependence of hPRL cellular function on pH.

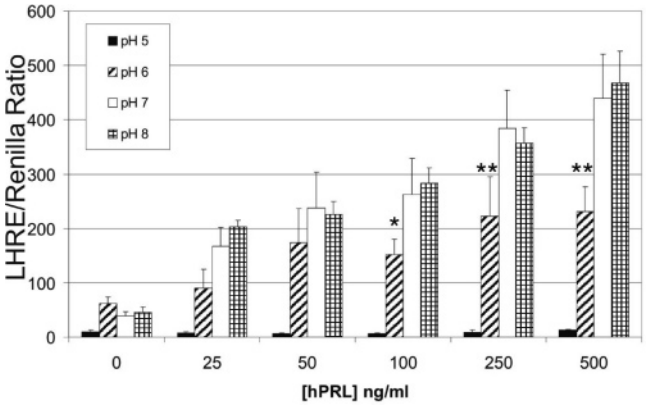


FIGURE 9: Effect of pH-adjusted media on STAT5-mediated gene transcription. T47D cells were cotransfected with LHRE-TK-Luc and *Renilla* (control) constructs and treated with increasing doses of hPRL in medium adjusted for pH (as labeled on the figure). Experimental results are presented as the ratio of luciferase/*Renilla* activity. Error bars indicate the standard deviation of three independent replicates. * indicates $p < 0.05$ and ** indicates $p < 0.001$ statistical significance between pH 7/8 and pH 6 at 100, 250, and 500 ng/mL doses, respectively.

*hPRL Stimulation of STAT5 Signaling in T47D Cells Is pH-Dependent.* Although the Nb2 assay is widely utilized, one valid concern involves the interspecies assay of PRL function (i.e., human PRL binding to rat PRLr). To both allay this concern and confirm the above biologic data with an alternative methodology, the pH dependence of the hPRL-induced activation of the STAT5 transcription factor in the human breast cancer cell line T47D was assessed (Figure 9). This was accomplished by the transfection of a STAT5-responsive luciferase construct, followed by incubation of the transfectants at various pH values in the presence of varying concentrations of hPRL. hPRL-stimulated transfectants incubated at pH 7.0−8.0 revealed a dose-dependent increase in STAT5-mediated luciferase gene transcription, with a 5-fold relative increase in luciferase activity at a dose of 500 ng/mL compared to untreated samples. In contrast, transfectants treated in medium adjusted to a pH of 6.0 demonstrated significantly lower relative STAT5-mediated luciferase activities at PRL concentrations of 100−500 ng/mL. As above, these data are consistent with our biophysical studies and suggest the possibility of a pH dependence to the biologic activity of hPRL. However, we recognize the limited scope of these initial bioassays and the caution required in their interpretation. The cellular response to variation in the extracellular pH is likely to reflect more than the pH dependence to binding of hPRL to its receptor. Future studies will be required to more completely define this complex phenomenon.

## DISCUSSION

To our knowledge, this publication presents the first evidence for pH dependence to both the structural stability and the receptor-binding properties of hPRL. The pattern of NMR chemical shift changes and amide HX rates along the hPRL backbone, along with surface electrostatic potential calculations, suggests a central role for a cluster of three His residues (27, 30, and 180) in the structural mechanism for this pH-dependent behavior. Located at the interface of the first and fourth α-helices, this cluster of His side chains is part of the high-affinity binding site for the hPRL receptor.

Because this variation in structural and functional properties occurs over the physiologic range from approximately pH 6.0 to pH 8.0, we consider below the potential spectrum of acidity changes that a hormone such as hPRL may experience in the human body and how its biologic behavior may be affected.

Immediately after synthesis in the pituitary, hPRL is packaged into secretory granules. This process is preceded by acidification of the trans-Golgi to around pH 6.0, where hPRL has been previously concentrated. Research suggests that the sudden decrease in pH, along with the consequences of protein crowding and the influx of $Zn^{2+}$, serves as a primary trigger for the reversible aggregation of hPRL into large-scale particles around which secretory granules are ultimately formed (*34*, *35*). Although it is possible that the observed changes in hPRL structural stability relate to this process, the appropriateness of the association is less clear as hGH storage would be expected to proceed similarly, yet hGH did not display the same pH-dependent changes in its global stability. However, we do note a subtle feature of the unfolding curves displayed in Figure 1. In both denaturants, hGH displays pH dependence to its fluorescence at low denaturant concentrations. This effect is more pronounced in guanidine, where a pre-unfolding conformational transition is visible, which becomes more pronounced at lower pH. Although the significance of this is unclear, it could suggest a pH-dependent structural change in native hGH that promotes reversible aggregation at lower pH. hGH is known to undergo a conformational change at low pH values ($<4$), which maintains its overall structural integrity and is not associated with complete denaturation (*36*). It is also important to note that functional and biochemical differences in the cellular storage of prolactin and growth hormone have been noted (*37*−*40*), which may also relate to the differences in behavior reported here. Regardless, surface electrostatic changes due to protonation of specific His residues are likely to play an important role in the cellular mechanism for storage of both hPRL and hGH into secretory granules.

We next consider the fate of extracellular hPRL after it is endocytosed at the cell surface as a consequence of receptor binding and activation. It has been well-established that, after internalization, the contents of endosomes are acidified to a pH between 5.5 and 6.5, depending on the maturation state of the organelle (*41*). The data reported here predict that hPRL will become largely dissociated from its receptor under these conditions. There are multiple possible biological implications of this effect. First, although not yet directly demonstrated for the hPRLr, many cytokine receptors continue to signal after endocytosis (*42*, *43*), which can significantly contribute to the overall cellular response. Dissociation of hPRL from its receptor may terminate any potential signaling of its receptor from the endocytic compartment. In contrast, hGH bound to the hPRLr might be expected to continue to signal endosomally due to a lack of pH-induced dissociation from the hPRLr. Second, the prototypical fates of endocytosed ligand−receptor complexes are for the dissociated ligand to be largely trafficked to lysosomes for eventual degradation and the empty membrane-spanning receptor to be recycled back to the cell surface. The pH-induced dissociation of ligand from the receptor represents a fundamental step in this process (*44*) but has not been specifically described for hPRL, and for most cytokine-receptor interactions the structural mechanism for the pH-dependent dissociation is not known. For the epidermal growth factor receptor, the varying pH dependence of dissociation for a number of ligands has been correlated with the degree of recycling (*45*, *46*) and, also, for insulin control of endosomal pH regulates intracellular signaling, degradation, and receptor recyling (*47*−*49*). It is possible that hPRL recycling is similarly modulated by the pH dependence of receptor dissociation. Lastly, endocytosed hPRL traffics via retrograde translocation through the endoplasmic reticulum into the nucleus (*7*, *24*, *50*, *51*), in a process involving association of hPRL with cyclophilin B. In the nucleus, the hPRL−cyclophilin B complex contributes to overall hPRL-induced signaling by catalyzing the release of inhibitory PIAS3 from dimers of STAT5. Again, the pH-induced dissociation of hPRL from its receptor may play a fundamental role in this process.

Although the pH of circulating blood is tightly controlled over a narrow range (7.35−7.45), the pH of extracellular fluid in the extravascular space varies more widely. In a commentary, Gerweck (*52*) reviews evidence for variation in the pH of extracellular fluids and finds a range of experimentally determined pH values for benign tissue from 7.1 to 7.7. Additionally, the measured extracellular pH of tumors and malignant tissue has been consistently found to be lower than the surrounding tissue, with acidities frequently in the pH range of 6.5−7.0. Therefore, a tumor-to-tissue pH gradient exists corresponding to the variation in hPRL structural and functional properties described here. It is possible that the overall behavior of hPRL differs in the tumor microenvironment due to this decreased pH. It is important to note that hPRL function has been implicated in the growth and development of multiple malignancies (*2*, *53*) and, in particular, to play an important role in breast cancer (*7*, *54*, *55*). The functional studies reported here may suggest that hPRL acts as a less effective agonist in tumors due to the decreased affinity for its receptor seen at lower pH. However, it is difficult to extrapolate our *in vitro* results to the much more complex milieu of tissue, where many additional factors are likely to exist.

PRL, studied in a number of animal species, is widely believed to exist in a variety of covalently modified forms, including glycosylated, phosphorylated, and proteolytically cleaved variants (*9*, *56*−*58*). The precise origin of the enzymatic activity responsible for these modifications is not well understood. However, it is possible that structural destabilization of PRL at lower pH described here plays an important role in this process. If access to an enzymatic active site is dependent on structural fluctuations in PRL, i.e., if local unfolding of ordered structure is required, then a large increase in the reaction rate may be induced by a relatively minor decrease in structural stability. This effect results from the 10-fold increase in the population of the unfolded state, which is directly accessible to enzymatic action, due to only unit changes in the $\Delta G_{unf}$. Although possible for any protein modification, this phenomenon occurs most frequently with site-specific proteolytic cleavage. A widely studied and fascinating variant of PRL is the so-called "16k-PRL", which is an N-terminal, 16 kDa proteolytic fragment of the hormone (*59*−*61*). 16k-PRL is potently antiangiogenic and appears to function through a cell-surface receptor that is independent of the PRLr. This variant can be produced in various ways,

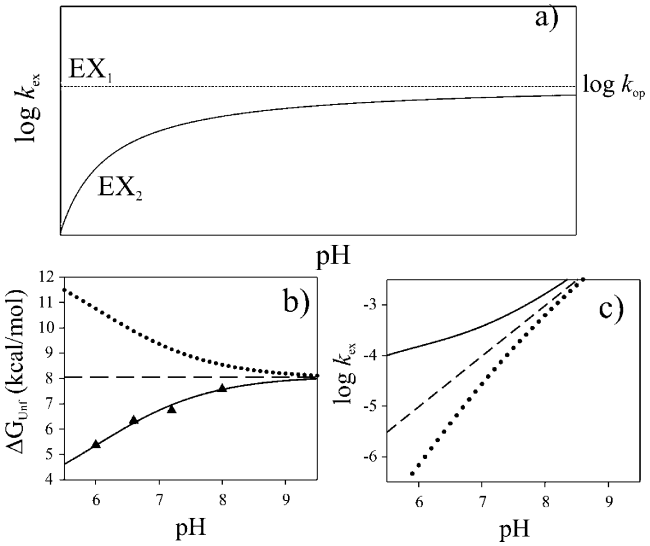


FIGURE 10: (a) The theoretical relationship between the measured amide hydrogen exchange rate, $k_{ex}$, and pH is displayed. (b) Three potential dependencies of global unfolding on pH, with experimental $\Delta G_{unf}$ values for hPRL (Figure 1) represented by triangles. The dotted and solid lines represent proteins with increased and decreased global stabilities with decreasing pH, respectively, whereas the dashed line represents a protein with no change in stability. (c) Expected relationship between log($k_{ex}$) values and pH, assuming pure $EX_2$ behavior, for the three possible dependencies of global stability on pH. The dashed line represents the expected linear behavior for a protein with no dependence of its global stability on pH, whereas the dotted and solid lines represent deviations from idealized behavior due to increasing and decreasing global stabilities with decreasing pH, respectively.

all of which cleave the protein in the second long loop between the third and fourth long helices. Subsequently, generation of active 16k-PRL also requires reduction of a disulfide bridge connecting the C-terminal α-helix with the N-terminal proteolytic fragment. Although the loop targeted for proteolytic cleavage is not highly ordered structurally under native conditions, some additional degree of unfolding may be required for optimal access to the protease. In the future, it will be interesting to consider the pH dependence of PRL proteolytic cleavage, especially once the endogenous protease responsible for generation of 16k-PRL has been identified.

Another potential consideration is the susceptibility of PRL to phosphorylation. Although controversial, a phosphorylated variant of hPRL involving Ser-179 has been described and extensively investigated (*62*−*64*). In animal studies, the pseudophosphorylated mutant S179D-hPRL appears to counter the tumorigenic activities of the wild-type protein (*65*−*68*) and has more recently been demonstrated to be potently antiangiogenic (*69*) and to induce apoptosis of endothelial cells (*70*). It is interesting to note that the cluster of three His residues (27, 30, and 180) implicated in the pH-dependent changes reported here is spatially adjacent to this site of modification. Because Ser-179 is buried within the hydrophobic core of the helical bundle, the structural mechanism for phosphorylation has always been unclear. Although only a speculation, it is possible that decreased pH locally destabilizes this region of the helical bundle in order to provide access to the target site for phosphorylation.

## ACKNOWLEDGMENT

We gratefully acknowledge the technical assistance from Mr. Syrus Meshack and helpful discussions with Drs. Andy Robertson and Priscilla Dannies. The bacterial expression vector for hGH production was a gift of Dr. Priscilla Dannies. We thank Dr. Gerald Shulman for use of his Hitachi H-3010 fluorescence spectrophotometer.

## APPENDIX

The relationship between hydrogen exchange and protein structure is described by a local unfolding model in which amide proton transfer is regulated by the equilibrium constant for local unfolding reactions. In such a model, the hydrogen exchange process only occurs when an amide proton is not involved in an intramolecular H-bond and is available for reaction with a solvent catalyst. Amide proton exchange is catalyzed only by the hydroxide ion above approximately pH 4. We define $K_{op}$ as the opening equilibrium constant for a particular protein ($K_{op} = k_{op}/k_{cl}$, where $k_{op}$ and $k_{cl}$ and the opening and closing kinetic rate constants, respectively) and $k_{ex}$ as the observed exchange rate for the amide proton of the protein backbone. The kinetic expression for proton exchange that is dependent on a structural isomerization or the breaking of an intramolecular H-bond preventing exchange is written as

$$k_{ex} = \frac{k_{op}k_{ch}[Cat]}{k_{cl} + k_{ch}[Cat]}$$

The "intrinsic" or "chemical" pseudo-first-order rate constant for exchange, dependent on a concentration of catalyst, is $k_{ch}$. When the closing rate is much lower than the chemical exchange rate ($k_{cl} \ll k_{ch}$), the above expression is reduced to

$$k_{ex} = k_{op}$$

and the observed amide proton exchange rate shows no dependence on pH. This is known as the so-called $EX_1$ condition or unimolecular exchange condition and is typically encountered at higher pH. In this exchange regime, experimentally derived exchange rates can be directly related to opening rates along a protein backbone. In the case where the re-formation of the H-bond that is responsible for protecting an amide from proton exchange is faster than the chemical exchange rate for the unprotected amide ($k_{cl} \gg k_{ch}$), the aforementioned kinetic expression is reduced to

$$k_{ex} = K_{op}k_{ch}[OH^-]$$

where $K_{op} = k_{op}/k_{cl}$. This is known as the $EX_2$ condition or the bimolecular exchange condition and is expected to occur at lower pH. Experimental exchange data collected under $EX_2$ conditions can be used to derive the equilibrium constant of structural isomerization on a per-residue basis and can be further related to the Gibbs free energy of stabilization. The free energy of stabilization for the closed form of the segment preventing exchange is calculated from the equilibrium constant:

$$\Delta G^0_{HX} = -RT \ln K_{op} = -RT \ln(k_{ex}/k_{ch}[OH^-])$$

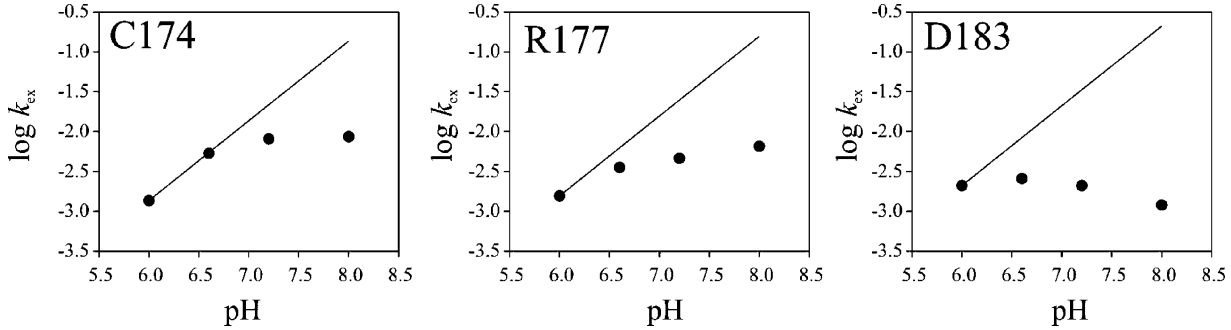


FIGURE 11: Measured backbone amide hydrogen exchange rates for three selected residues as a function of pH (circles). In each case, the solid line represents the linear trend expected for pure $EX_2$ behavior, assuming no pH dependence of global unfolding.

The generalized behavior of the HX exchange as a function of pH for a folded protein is illustrated in Figure 10a, where pure $EX_1$ behavior is traced by a dotted line and $EX_2$ by a solid line. The relationship between pH and amide hydrogen exchange depicted in Figure 10a is developed under the assumption that the protein being studied has a constant structural stability over the indicated pH range. A hypothetical pH-dependent stability profile for hPRL is represented by the solid line in Figure 10b. This line traces the empirically determined $\Delta G_U$ values (solid triangles) for hPRL reported in Figure 1. For the purpose of comparison, traces representing a protein showing no pH dependence on stability (dashed line) and a decreasing stability at higher pH values (dotted line) are also shown in Figure 10b. The reduction in global stability for hPRL would be expected to increase $K_{op}$ and the measured exchange rate at lower pH values. The general effects of pH dependence on the NMR-determined amide exchange rates for protons under the $EX_2$ condition are illustrated in Figure 10c. The three stability profiles of Figure 10b were used to calculate the three curves in Figure 10c, each representing a different pH dependence of $EX_2$ exchange (ignoring the transition to $EX_1$). A typical experimental protocol for distinguishing $EX_1$ from $EX_2$ behavior is to measure observed HX rates across a range of pH values. When a linear relationship between log($k_{ex}$) and pH is noted, similar to the dashed line in Figure 10c, $EX_2$ behavior can be presumed. At higher pH values, where measured log($k_{ex}$) values become pH-independent, $EX_1$ behavior is evident. However, when either local or global unfolding reactions are pH-dependent, identification of the precise transition between $EX_2$ and $EX_1$ behavior becomes problematic, due to the deviations from a unitary slope in the low-pH portion of log($k_{ex}$) versus pH plots (i.e., the region representing pure $EX_2$ behavior in Figure 10a).

Figure 11 depicts the NMR-based HX exchange data measured at pH 6.0, 6.6, 7.2, and 8.0 for three selected residues in hPRL. In each graph, solid circles represent the experimentally derived data, and the solid line represents the linear trend expected for pure $EX_2$ exchange behavior expected at low pH, assuming no pH dependence of unfolding/opening. All three of the selected residues are buried within the hydrophobic of the helical bundle, and exchange of their amide hydrogens would be expected to depend primarily on global unfolding reactions. C174 displays what appears to be nearly ideal behavior for a residue showing little or no pH dependence on its localized stability and transitions appropriately from $EX_2$ to $EX_1$ behavior around pH 7.5. However, a majority of residues in hPRL show significant deviations from ideal behavior similar to residues R177 and D183 in Figure 11. Despite the difficulty in clearly discerning $EX_1$ and $EX_2$ behavior, HX data for hPRL have been analyzed assuming $EX_2$ behavior at pH 6.6 and below. The average $\Delta G_{HX}$ values for the helical bundle reported in Table 1, derived assuming $EX_1$ behavior at pH 6.6, are within 1 kcal/mol of the reported $\Delta G_{unf}$ determined by urea denaturation, supporting the validity of this assumption. We chose to assume $EX_1$ behavior for all residues at pH 8.0 based on the apparent flattening of their HX rates at pH 7.5 and above, similar to C174 in Figure 11, for a subset of residues. Currently, we do not have independent measurements of global unfolding rates for hPRL to compare to localized $k_{op}$ values as a potential means for confirming $EX_1$ behavior. We accept that the assumption of $EX_2$ and $EX_1$ behavior at pH 6.6 and 8.0, respectively, may not apply to all residues in hPRL. We only assert that at these two limits of pH, in each case, a majority of residues follow the ascribed behavior and, therefore, only general trends in local backbone stability and opening kinetics can be reliably interpreted.

## REFERENCES

1. Wells, J. A., and de Vos, A. M. (1996) Hematopoietic receptor complexes, *Annu. Rev. Biochem. 65*, 609−634.
2. Ben-Jonathan, N., Liby, K., McFarland, M., and Zinger, M. (2002) Prolactin as an autocrine/paracrine growth factor in human cancer, *Trends Endocrinol. Metab. 13*, 245−250.
3. Leav, I., Merk, F. B., Lee, K. F., Loda, M., Mandoki, M., McNeal, J. E., and Ho, S. M. (1999) Prolactin receptor expression in the developing human prostate and in hyperplastic, dysplastic, and neoplastic lesions, *Am. J. Pathol. 154*, 863−870.
4. Clevenger, C. V., Chang, W. P., Ngo, W., Pasha, T. L. M., Montone, K. T., and Tomaszewski, J. E. (1995) Expression of prolactin and prolactin receptor in human breast-carcinoma—evidence for an autocrine paracrine loop, *Am. J. Pathol. 146*, 695−705.
5. Reynolds, C., Montone, K. T., Powell, C. M., Tomaszewski, J. E., and Clevenger, C. V. (1997) Expression of prolactin and its receptor in human breast carcinoma, *Endocrinology 138*, 5555−5560.
6. Maus, M. V., Reilly, S. C., and Clevenger, C. V. (1999) Prolactin as a chemoattractant for human breast carcinoma, *Endocrinology 140*, 5447−5450.
7. Clevenger, C. V., Furth, P. A., Hankinson, S. E., and Schuler, L. A. (2003) The role of prolactin in mammary carcinoma, *Endocr. Rev. 24*, 1−27.
8. Ben-Jonathan, N., Mershon, J. L., Allen, D. L., and Steinmetz, R. W. (1996) Extrapituitary prolactin: distribution, regulation, functions, and clinical aspects, *Endocr. Rev. 17*, 639−669.
9. Sinha, Y. N. (1995) Structural variants of prolactin—occurrence and physiological significance, *Endocr. Rev. 16*, 354−369.
10. Schroeder, M. D., Brockman, J. L., Walker, A. M., and Schuler, L. A. (2003) Inhibition of prolactin (PRL)-induced proliferative

signals in breast cancer cells by a molecular mimic of phosphorylated PRL, S179D-PRL, *Endocrinology 144*, 5300−5307.
11. Wu, W., Coss, D., Lorenson, M. Y., Kuo, C. B., Xu, X., and Walker, A. M. (2003) Different biological effects of unmodified prolactin and a molecular mimic of phosphorylated prolactin involve different signaling pathways, *Biochemistry 42*, 7561−7570.
12. Xu, X., Wu, W., Williams, V., Khong, A., Chen, Y. H., Deng, C., and Walker, A. M. (2003) Opposite effects of unmodified prolactin and a molecular mimic of phosphorylated prolactin on morphology and the expression of prostate specific genes in the normal rat prostate, *Prostate 54*, 25−33.
13. Corbacho, A. M., Nava, G., Eiserich, J. P., Noris, G., Macotela, Y., Struman, I., de la Martinez, E. G., Freeman, B. A., and Clapp, C. (2000) Proteolytic cleavage confers nitric oxide synthase inducing activity upon prolactin, *J. Biol. Chem. 275*, 13183−13186.
14. D'Angelo, G., Martini, J. F., Iiri, T., Fantl, W. J., Martial, J., and Weiner, R. I. (1999) 16K human prolactin inhibits vascular endothelial growth factor-induced activation of Ras in capillary endothelial cells, *Mol. Endocrinol. 13*, 692−704.
15. Clapp, C., Martial, J. A., Guzman, R. C., Rentier-Delure, F., and Weiner, R. I. (1993) The 16-kilodalton N-terminal fragment of human prolactin is a potent inhibitor of angiogenesis, *Endocrinology 133*, 1292−1299.
16. Keeler, C., Dannies, P. S., and Hodsdon, M. E. (2003) The tertiary structure and backbone dynamics of human prolactin, *J. Mol. Biol. 328*, 1105−1121.
17. Teilum, K., Hoch, J. C., Goffin, V., Kinet, S., Martial, J. A., and Kragelund, B. B. (2005) Solution structure of human prolactin, *J. Mol. Biol. 351*, 810−823.
18. Bignon, C., Sakal, E., Belair, L., Chapnik-Cohen, N., Djiane, J., and Gertler, A. (1994) Preparation of the extracellular domain of the rabbit prolactin receptor expressed in *Escherichia coli* and its interaction with lactogenic hormones, *J. Biol. Chem. 269*, 3318−3324.
19. Pace, C. N., and Scholtz, J. M. (1997) Measuring the conformational stability of a protein, in *Protein Structure* (Creighton, T. E., Ed.) 2nd ed., pp 299−321, Oxford University Press, Oxford.
20. Delaglio, F., Grzesiek, S., Vuister, G. W., Zhu, G., Pfeifer, J., and Bax, A. (1995) NMRPipe—a multidimensional spectral processing system based on Unix Pipes, *J. Biomol. NMR 6*, 277−293.
21. Kneller, D. G., and Goddard, T. D. (1997) SPARKY, University of California, San Francisco.
22. Cavanagh, J. (1996) Referencing, in *Protein NMR spectroscopy: Principles and Practice*, pp 175−176, Academic Press, San Diego.
23. Glasoe, P. K., and Long, F. A. (1960) Use of glass electrodes to measure acidities in deuterium oxide, *J. Phys. Chem. 64*, 188−190.
24. Rycyzyn, M. A., and Clevenger, C. V. (2002) The intranuclear prolactin/cyclophilin B complex as a transcriptional inducer, *Proc. Natl. Acad. Sci. U.S.A. 99*, 6790−6795.
25. DeFelippis, M. R., Kilcomons, M. A., Lents, M. P., Youngman, K. M., and Havel, H. A. (1995) Acid stabilization of human growth hormone equilibrium folding intermediates, *Biochim. Biophys. Acta 1247*, 35−45.
26. Kinet, S., Goffin, V., Mainfroid, V., and Martial, J. A. (1996) Characterization of lactogen receptor-binding site 1 of human prolactin, *J. Biol. Chem. 271*, 14353−14360.
27. Yang, A. S., and Honig, B. (1993) On the pH dependence of protein stability, *J. Mol. Biol. 231*, 459−474.
28. Englander, S. W., and Krishna, M. M. (2001) Hydrogen exchange, *Nat. Struct. Biol. 8*, 741−742.
29. Englander, S. W., Sosnick, T. R., Englander, J. J., and Mayne, L. (1996) Mechanisms and uses of hydrogen exchange, *Curr. Opin. Struct. Biol. 6*, 18−23.
30. Englander, S. W., and Kallenbach, N. R. (1983) Hydrogen exchange and structural dynamics of proteins and nucleic acids, *Q. Rev. Biophys. 16*, 521−655.
31. Huyghues-Despointes, B. M., Pace, C. N., Englander, S. W., and Scholtz, J. M. (2001) Measuring the conformational stability of a protein by hydrogen exchange, *Methods Mol. Biol. 168*, 69−92.
32. Englander, S. W. (2000) Protein folding intermediates and pathways studied by hydrogen exchange, *Annu. Rev. Biophys. Biomol. Struct. 29*, 213−238.
33. Gout, P. W., Beer, C. T., and Noble, R. L. (1980) Prolactin-stimulated growth of cell cultures established from malignant Nb rat lymphomas, *Cancer Res. 40*, 2433−2436.
34. Dannies, P. S. (2002) Mechanisms for storage of prolactin and growth hormone in secretory granules, *Mol. Genet. Metab. 76*, 6−13.
35. Sankoorikal, B. J., Zhu, Y. L., Hodsdon, M. E., Lolis, E., and Dannies, P. S. (2002) Aggregation of human wild-type and H27A-prolactin in cells and in solution: Roles of $Zn^{2+}$, $Cu^{2+}$, and pH, *Endocrinology 143*, 1302−1309.
36. Kasimova, M. R., Kristensen, S. M., Howe, P. W., Christensen, T., Matthiesen, F., Petersen, J., Sorensen, H. H., and Led, J. J. (2002) NMR studies of the backbone flexibility and structure of human growth hormone: a comparison of high and low pH conformations, *J. Mol. Biol. 318*, 679−695.
37. Lorenson, M. Y., and Jacobs, L. S. (1982) Thiol regulation of protein, growth hormone, and prolactin release from isolated adenohypophysial secretory granules, *Endocrinology 110*, 1164−1172.
38. Lorenson, M. Y., Robson, D. L., and Jacobs, L. S. (1983) Divalent cation inhibition of hormone release from isolated adenohypophysial secretory granules, *J. Biol. Chem. 258*, 8618−8622.
39. Slaby, F., and Farquhar, M. G. (1980) Characterization of rat somatotroph and mammotroph secretory granules. Presence of sulfated molecules, *Mol. Cell. Endocrinol. 18*, 33−48.
40. Lorenson, M. Y., Patel, T., Liu, J. W., and Walker, A. M. (1996) Prolactin (PRL) is a zinc-binding protein. I. Zinc interactions with monomeric PRL and divalent cation protection of intragranular PRL cysteine thiols, *Endocrinology 137*, 809−816.
41. Mellman, I., Fuchs, R., and Helenius, A. (1986) Acidification of the endocytic and exocytic pathways, *Annu. Rev. Biochem. 55*, 663−700.
42. Polo, S., and Di Fiore, P. P. (2006) Endocytosis conducts the cell signaling orchestra, *Cell 124*, 897−900.
43. Le, R. C., and Wrana, J. L. (2005) Clathrin- and non-clathrin-mediated endocytic regulation of cell signaling, *Nat. Rev. Mol. Cell Biol. 6*, 112−126.
44. Mellman, I., Fuchs, R., and Helenius, A. (1986) Acidification of the endocytic and exocytic pathways, *Annu. Rev. Biochem. 55*, 663−700.
45. French, A. R., Tadaki, D. K., Niyogi, S. K., and Lauffenburger, D. A. (1995) Intracellular trafficking of epidermal growth factor family ligands is directly influenced by the pH sensitivity of the receptor/ligand interaction, *J. Biol. Chem. 270*, 4334−4340.
46. Lauffenburger, D. A., Fallon, E. M., and Haugh, J. M. (1998) Scratching the (cell) surface: cytokine engineering for improved ligand/receptor trafficking dynamics, *Chem. Biol. 5*, R257−R263.
47. Balbis, A., Baquiran, G., Dumas, V., and Posner, B. I. (2004) Effect of inhibiting vacuolar acidification on insulin signaling in hepatocytes, *J. Biol. Chem. 279*, 12777−12785.
48. Posner, B. I. (2003) Regulation of insulin receptor kinase activity by endosomal processes: possible areas for therapeutic intervention, *Curr. Opin. Invest. Drugs 4*, 430−434.
49. Bevan, A. P., Seabright, P. J., Tikerpae, J., Posner, B. I., Smith, G. D., and Siddle, K. (2000) The role of insulin dissociation from its endosomal receptor in insulin degradation, *Mol. Cell. Endocrinol. 164*, 145−157.
50. Rycyzyn, M. A., and Clevenger, C. V. (2000) Role of cyclophilins in somatolactogenic action, *Neuroimmunomodulation 917*, 514−521.
51. Rycyzyn, M. A., Reilly, S. C., O'Malley, K., and Clevenger, C. V. (2000) Role of cyclophilin B in prolactin signal transduction and nuclear retrotranslocation, *Mol. Endocrinol. 14*, 1175−1186.
52. Gerweck, L. E. (2000) The pH difference between tumor and normal tissue offers a tumor specific target for the treatment of cancer, *Drug Resist. Updates 3*, 49−50.
53. Goffin, V., Binart, N., Touraine, P., and Kelly, P. A. (2002) Prolactin: The new biology of an old hormone, *Annu. Rev. Physiol. 64*, 47−67.
54. Goffin, V., Touraine, P., Pichard, C., Bernichtein, S., and Kelly, P. A. (1999) Should prolactin be reconsidered as a therapeutic target in human breast cancer?, *Mol. Cell. Endocrinol. 151*, 79−87.
55. Llovera, M., Touraine, P., Kelly, P. A., and Goffin, V. (2000) Involvement of prolactin in breast cancer: redefining the molecular targets, *Exp. Gerontol. 35*, 41−51.
56. Schenck, E. J., Canfield, J. M., and Brooks, C. L. (2003) Functional relationship of serine 90 phosphorylation and the surrounding putative salt bridge in bovine prolactin, *Mol. Cell. Endocrinol. 204*, 117−125.
57. Gonzalez, C., Corbacho, A. M., Eiserich, J. P., Garcia, C., Lopez-Barrera, F., Morales-Tlalpan, V., Barajas-Espinosa, A., az-Munoz,

M., Rubio, R., Lin, S. H., de la Martinez, E. G., and Clapp, C. (2004) 16K-prolactin inhibits activation of endothelial nitric oxide synthase, intracellular calcium mobilization, and endothelium-dependent vasorelaxation, *Endocrinology 145*, 5714−5722.

58. Tan, D., Johnson, D. A., Wu, W., Zeng, L., Chen, Y. H., Chen, W. Y., Vonderhaar, B. K., and Walker, A. M. (2005) Unmodified prolactin (PRL) and S179D PRL-initiated bioluminescence resonance energy transfer between homo- and hetero-pairs of long and short human PRL receptors in living human cells, *Mol. Endocrinol. 19*, 1291−1303.
59. Aranda, J., Rivera, J. C., Jeziorski, M. C., Riesgo-Escovar, J., Nava, G., Lopez-Barrera, F., Quiroz-Mercado, H., Berger, P., de la Martinez, E. G., and Clapp, C. (2005) Prolactins are natural inhibitors of angiogenesis in the retina, *Invest. Ophthalmol. Visual Sci. 46*, 2947−2953.
60. Macotela, Y., Mendoza, C., Corbacho, A. M., Cosio, G., Eiserich, J. P., Zentella, A., Martinez de la Escalera, G., and Clapp, C. (2002) 16K prolactin induces NF-kappaB activation in pulmonary fibroblasts, *J. Endocrinol. 175*, 13−18.
61. Bentzien, F., Struman, I., Martini, J. F., Martial, J., and Weiner, R. (2001) Expression of the antiangiogenic factor 16K hPRL in human HCT116 colon cancer cells inhibits tumor growth in Rag1-(−/−) mice, *Cancer Res. 61*, 7356−7362.
62. Walker, A. M. (2005) Prolactin receptor antagonists, *Curr. Opin. Invest. Drugs 6*, 378−385.
63. Chen, T. J., Kuo, C. B., Tsai, K. F., Liu, J. W., Chen, D. Y., and Walker, A. M. (1998) Development of recombinant human prolactin receptor antagonists by molecular mimicry of the phosphorylated hormone, *Endocrinology 139*, 609−616.
64. Wang, Y. F., Liu, J. W., Mamidi, M., and Walker, A. M. (1996) Identification of the major site of rat prolactin phosphorylation as serine 177, *J. Biol. Chem. 271*, 2462−2469.
65. Schroeder, M. D., Brockman, J. L., Walker, A. M., and Schuler, L. A. (2003) Inhibition of prolactin (PRL)-induced proliferative signals in breast cancer cells by a molecular mimic of phosphorylated PRL, S179D-PRL, *Endocrinology 144*, 5300−5307.
66. Xu, X., Wu, W., Williams, V., Khong, A., Chen, Y. H., Deng, C., and Walker, A. M. (2003) Opposite effects of unmodified prolactin and a molecular mimic of phosphorylated prolactin on morphology and the expression of prostate specific genes in the normal rat prostate, *Prostate 54*, 25−33.
67. Kuo, C. B., Wu, W., Xu, X., Yang, L., Chen, C., Coss, D., Birdsall, B., Nasseri, D., and Walker, A. M. (2002) Pseudophosphorylated prolactin (S179D PRL) inhibits growth and promotes beta-casein gene expression in the rat mammary gland, *Cell Tissue Res. 309*, 429−437.
68. Xu, X., Kreye, E., Kuo, C. B., and Walker, A. M. (2001) A molecular mimic of phosphorylated prolactin markedly reduced tumor incidence and size when DU145 human prostate cancer cells were grown in nude mice, *Cancer Res. 61*, 6098−6104.
69. Ueda, E., Ozerdem, U., Chen, Y. H., Yao, M., Huang, K. T., Sun, H., Martins-Green, M., Bartolini, P., and Walker, A. M. (2006) A molecular mimic demonstrates that phosphorylated human prolactin is a potent anti-angiogenic hormone, *Endocr. Relat. Cancer 13*, 95−111.
70. Ueda, E. K., Lo, H. L., Bartolini, P., and Walker, A. M. (2006) S179D Prolactin (PRL) primarily uses the extrinsic pathway and MAPkinase signaling to induce apoptosis in human endothelial cells, *Endocrinology*.

BI061958V